Supplementary Materials for

A 12 Å carotenoid translocation in a photoswitch associated with cyanobacterial photoprotection

Ryan L. Leverenz, Markus Sutter, Adjélé Wilson, Sayan Gupta, Adrien Thurotte, Céline Bourcier de Carbon, Christopher J. Petzold, Corie Ralston, François Perreau, Diana Kirilovsky, Cheryl A. Kerfeld*

*Corresponding author. E-mail: ckerfeld@lbl.gov

Published 26 June 2015, *Science* **348**, 1463 (2015)
DOI: 10.1126/science.aaa7234

This PDF file includes:

Materials and Methods

Construction of the RCP plasmid for expression in *E. coli*

To obtain the NTD/RCP of *Synechocystis* OCP, we cloned a C-terminal His-tagged *Synechocystis* OCP in a pCDFDuet-1 plasmid creating the plasmid pCDF-OCPsynCtag as previously described (*31*). To obtain the pCDF-RCP-Syn-1-165Ctag plasmid, the nucleotides encoding the last 169 amino acids (CTD) of the *ocp* gene were deleted by site-directed mutagenesis using the plasmid pCDF-OCPsynCtag as template and synthetic primers (table S6A). The deletion of the nucleotides coding for the first 20 amino acids of the RCP was obtained using the pCDF-RCP-Syn-1-165Ctag as template and the synthetic primers (table S6B) to obtain the plasmid pCDF-RCP-Syn-20-165-Ctag.

Site-directed mutagenesis

The point mutations P126, Y129, P126/Y129, E34 and C84 were introduced by directed mutagenesis, using the pCDF-Syn-3aaNtag plasmid as template and mismatching primers (table S6C). When possible, restriction sites were added by silent mutation (Mfe for P126, Y129 and P126Y129 or XmaI for C84A) to check the presence of the point mutations. Sequencing of the cloned gene confirmed the presence of the mutations and the absence of unwanted mutations.

Holoprotein production in *E. coli*

E. coli BL21-Gold (DE3) cells from Agilent Technologies were used for OCP/RCP production. BL21 cells were transformed simultaneously with three plasmids: (1) pAC-BETA (described previously (*32*)), containing the CrtB-CrtE-CrtI, CrtY operon need to synthesize β-carotene (2) pBAD-CrtO or pBAD-CrtW (CrtO and CrtW catalyze mainly the transformation of β-carotene into echinenone and canthaxanthin, respectively), and (3) pCDF-OCP or pCDF-RCP plasmids, containing *Synechocystis ocp* or *rcp* genes, respectively. The construction of pBAD-CrtO, pBAD-CrtW and pCDF-OCP is described elsewhere (*31*). Transformed cells were grown in the presence ampicillin (50 µg/ml), chloramphenicol (17 µg/ml), and streptomycin (25 µg/ml). For induction of the different genes, transformed *E. coli* cells were grown in TB medium at 37°C for 3-4 hours until OD_{600}=0.8, at which point arabinose was added (0.02%). Following overnight growth at 37°C, cell cultures were diluted with fresh medium and arabinose (0.02%) and grown at 37°C until OD_{600} = 1-1.2. Isopropyl β-D-thiogalactoside (IPTG) (0.2 mM) was added and the cells incubated overnight at 28°C. In the morning, the cultures were harvested and pellets were stored at -80°C until used for protein purification.

Carotenoid content analysis

Carotenoids were extracted as described previously (*33*). Relative quantification of carotenoids was calculated using the results of liquid chromatography-mass spectrometry (LC-MS) analysis as described previously (*15*).

Purification of OCP and RCP holoproteins

His-tagged OCP overexpressed in *Synechocystis* were isolated as described previously (*12*). OCP and RCP expressed in *E. coli* were isolated as described elsewhere (*31*). Briefly, cells are resuspended in lysis buffer (40 mM Tris pH 8/10% glycerol/300mM NaCl/1mM EDTA/1mM PMSF, 1mM caproic acid/1mM benzamidic acid/ 50 μg mL^{-1}) were broken in dim light using a French press. The membranes were pelleted and the supernatant was loaded on a nickel affinity column (Ni-Probond resin, Invitrogen). OCP was eluted with 200 mM imidazole and then dialyzed against 40 mM Tris-HCl. Purification of OCP_{CAN} and RCP_{CAN} by affinity chromatography yielded a mixture of apo- and holo-proteins. The RCP_{CAN} holoprotein was isolated using a combination of hydrophobic interaction chromatography (HIC) and size exclusion chromatography (SEC). The OCP_{CAN} holoprotein was isolated by SEC alone. HIC was performed using a linearly decreasing $(NH_4)_2SO_4$ gradient (1.5 M to 0 M) to elute protein bound to a Toyopearl Super-Q 650-S Phenyl resin (Tosoh Biosciences, 1.5 cm D x 15 cm H resin bed dimensions). SEC was performed using isocratic elution (50 mM Tris-HCl, 200 mM NaCl mobile phase) on a HiLoad 16/60 Superdex-75 column (GE Healthcare).

Protein crystallization

The purified N-terminal His-tagged OCP and C-terminal His-tagged RCP holoproteins were exchanged into 10 mM Tris-HCl pH 7.4 and concentrated using centrifugal concentrators (Amicon 0.5, 10 kDa [EMD Millipore]) prior to crystallization. RCP_{CAN} (2 mg/mL) was crystallized at 22°C in sitting drops containing 2 μL of protein plus 1 μL of crystallization solution (100 mM citric acid BIS-TRIS propane pH 5.5, 24% poly-ethylene glycol 3350). OCP_{CAN} (3 mg/mL) was crystallized at 22°C in sitting drops containing 2 μL of protein plus 1 μL of crystallization solution (100 mM sodium acetate pH 4.5, 10% poly-ethylene glycol 20,000, 3% glycerol). Crystals were flash frozen in liquid nitrogen after being transferred to a cryoprotectant solution (crystallization solution plus 15% ethylene glycol for RCP_{CAN}; crystallization solution plus 30% glycerol for OCP_{CAN}).

Diffraction data collection, structure determination and visualization

Diffraction data were collected at the Advanced Light Source at Lawrence Berkeley National Laboratory beamline 5.0.2 (1 Å wavelength, 100K). Diffraction data were integrated with XDS (*34*) and scaled with SCALA (CCP4 (*35*)). The structure of RCP was solved by molecular replacement with phenix.mr_rosetta (*36*) with a starting model based on the N-terminal domain of OCP (PDB ID 3MG1). Refinement was performed with phenix.refine (*37*) alternating with model building using 2Fo-Fc and Fo-Fc maps visualized in COOT (*38*). 99% of the residues were in the favored region of the Ramachandran plot, and the remaining 1% were in the allowed region for both structures. Statistics for diffraction data collection, structure determination and refinement are summarized in Table S2. Figures of crystal structures were prepared using pymol (www.pymol.org) and UCSF Chimera molecular visualization software (*39*).

Structural Analysis

OCP and RCP structures were aligned in UCSF Chimera using the MatchMaker tool and default alignment parameters. The reported distance between the CAN chromophores in the two structures (12 Å) is the distance between the C6 carbons of the two CANs in the alignment (see fig. S1C for carbon numbering). Solvent accessibility of CAN was determined using the areaimol (*40*) program in CCP4 (*35*). Electrostatics calculations were done using the APBS plugin for PyMOL(*41*).

Primary Structure Analysis and Sequence Logo: A full-length OCP sequence logo was generated from a MUSCLE alignment of 168 OCP gene sequences from publicly available genomes in IMG (http://img.jgi.doe.gov). The logo was built using the WebLogo application (http://www.weblogo.berkeley.edu) (*42*).

UV-Visible spectroscopy and measurements of photochemical kinetics

Absorbance spectra, kinetics of photoactivity (illumination with 5000 µmol photons m^{-2} s^{-1} of white light) and dark recovery of the OCP were measured in a spectrophotometer Specord S600 (Analyticjena) at 9°C.

***In vitro* reconstitution of PB binding**

An *in vitro* reconstitution system allows us to monitor OCP to PBs binding by following the fluorescence across time (*13*). Fluorescence yield quenching was monitored using a pulse amplitude modulated fluorometer (101/102/103-PAM, Walz). Measurements were made in a 1-cm pathlength stirred cuvette. OCP was pre-converted to the OCP^R form by 10 min illumination with 5000 µmol photons m^{-2} s^{-1} of white light at 4°C. Then, the OCP^R (0.48 µM) or RCP (0.48 µM) was added to 0.012 µM of PBs in 0.8M and 1.4 M potassium phosphate buffer (pH=7.5) at 23°C under 900 µmol photons.$m^{-2}s^{-1}$ blue-green light (white light filtered by a Corion cutoff 550-nm filter; 400-550nm). The ratio of OCP^R (or RCP) to PB was = 40. The concentration of OCP (RCP) was calculated from the carotenoid absorbance spectra since only the OCP holoprotein can be photoactivated and bind to PBs ($A^{1\%}_{1cm}$ carotenoid = 2158). RCP isolated by native proteolysis of OCP (OCP from *Synechocystis* ΔCrtR cells) and used in *in-vitro* PB reconstitution experiments was purified as described previously (*16*).

X-ray hydroxyl radical footprinting and mass spectrometry

OCP_{CAN} and RCP_{CAN} (expressed in *E. coli*) were exchanged into 20 mM potassium phosphate (pH 7.4), 100 mM NaCl by SEC on a Superdex-75 10/300 GL column prior to XF-MS experiments. Prior to x-ray irradiation of OCP^R, the sample syringe was cooled with an ice pack and illuminated with a blue LED array (470 nm Luxeon Rebel, Philips Lumileds).

Protein samples were irradiated in the millisecond and microsecond time range at beamlines 3.2.1 and 5.3.1 at the Advanced Light Source as reported previously (*43*). All samples, including the control (no x-ray irradiation), were subjected to cys-alkylation and salt removal prior to overnight Trypsin and GluC digestion at pH 8 and 37 C. Proteolyzed samples were analyzed in an Agilent 6550 iFunnel Q-TOF mass spectrometer (Agilent Technologies, Santa Clara, CA) coupled to an Agilent 1290 LC system (Agilent) using Sigma-Aldrich Ascentis Peptides ES-C18 reverse phase column (2.1 mm x 100 mm, 2.7 µm particle size; Sigma- Aldrich, St. Louis, MO). Approximately 10 pmol of samples

were loaded onto the column via an Infinity Autosampler (Agilent) with Buffer A (2% Acetonitrile, 0.1% Formic Acid) flowing at 0.400 mL/min. The peptides were separated and eluted into the mass spectrometer via a gradient with initial condition of 5% buffer B (98% Acetonitrile, 0.1% Formic Acid) increasing to 70% B over 15 minutes. Subsequently, B was increased to 90% over 1 minute and held for 3 minutes at a flow rate of 0.6 ml/min followed by a ramp back down to 5% over 1 minute where it was held for minutes to re-equilibrate the column to the original condition. Peptides were introduced to the mass spectrometer from the LC using a Jet Stream source (Agilent) operating in positive-ion mode (3500 V). The data were acquired with MassHunter B.05.00 operating in Auto MS/MS mode whereby the three most intense ions (charge states 2 - 5) within 300 m/z to 1400 m/z mass range above a threshold of 1000 counts were selected for MS/MS analysis. MS/MS spectra were collected with the quadrupole set to "Narrow" resolution and collision energy to optimize fragmentation. MS/MS spectra were scanned from m/z 100 1700 and were collected until 40000 total counts were collected or for a maximum accumulation time of 333 ms. Parent ions were excluded for 0.1 minutes following MS/MS acquisition. MS/MS data of native and modified peptide fragments were interpreted by Mascot MS/MS Ions Search as well as verified manually. The abundance of native and modified peptides at any irradiation time point area were measured (peak area) from their respective extracted ion chromatogram using Agilent Mass Hunter Ver 2.0.

Data analysis and dose response plots: The peak area from the extracted ion chromatograms of a specific peptide fragment with a particular mass-to-charge ratio and associated +16-, +32- or +48- Da sidechain modifications was used to quantify the amount of modification at a given irradiation time (*21*). Increasing irradiation progressively reduces the fraction of unmodified products and provides a site-specific dose response plot (as in Figure 3A). The hydroxyl radical reactivity rate (*k*), which depends on both intrinsic reactivity and SA, was obtained by fitting the dose response to a single exponential decay (based on a pseudo-first-order reaction scheme using Origin 7.5 (OriginLabs®). The ratio (R) of the measured reactivity of the side chains residues between OCP^O - OCP^R ($R = k_{OCPO}/k_{OCPR}$) and OCP^O – RCP ($R = k_{OCPO}/k_{OCPR}$) gave information on SA changes independent of the intrinsic reactivity (*44*).

RCP-phycobilisome docking analysis

The RCP_{CAN} and $OCP^O{}_{CAN}$ were docked to the ApcAB (PDB ID 4F0U (*45*)) using half of an ApcAB trimer (1 ApcA and 2 ApcB) using rosetta-dock (*46*). Protein structures were energy minimized using the rosetta-relax application prior to the docking step. Unconstrained docking simulations were performed for 25'000 runs and the top 1000 docking solutions according to the Rosetta score functions were analyzed for carotenoid-bilin distances. When using constrained docking the C4 atom of the RCP CAN was restrained to O5 of ApcA using a harmonic function with x0=4 Å and a sd of 1 Å.

Fig. S1.

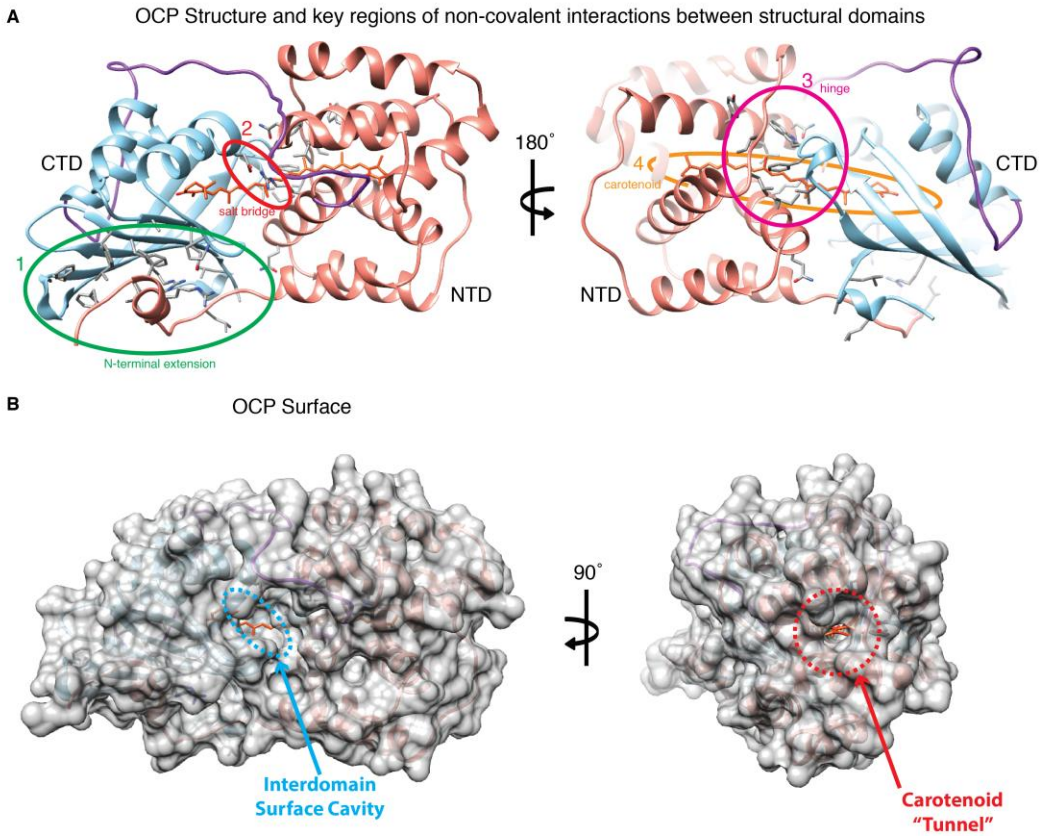

Figure S1. Views of OCP structure illustrating key NTD-CTD interactions and surface cavities. (**A**) Four primary regions of NTD/CTD interaction are indicated (circled) on the ribbon structures: 1.) the N-terminal extension (including the αA helix), which forms extensive H-bonding and non-bonding contacts to the CTD β-sheet (green circled area), 2.) the R155:E244 salt bridge (red circled area) observed at a large surface cleft between the NTD and CTD that exposes CAN to solvent, 3.) the putative W277 CTD hinge region dominated by hydrophobic contacts with the NTD and CAN (magenta circled area), 4.) the carotenoid chromophore, which is in extensive hydrophobic contact with residues in both domains and H-bonds to residues Y201 and W288 in the CTD. (**B**) CAN in OCP^O is solvent exposed primarily via a large surface cavity (circled in blue) at the NTD/CTD interface. A second solvent accessible region of CAN exists in the NTD near residues Y44 and W41.[25] A hydrophobic tunnel (its opening is circled in red) extends from the carotenoid to the surface of the N-terminal domain. Structures were modeled using OCP_{CAN} coordinates from this study (PDB ID 4XB5).

Fig. S1

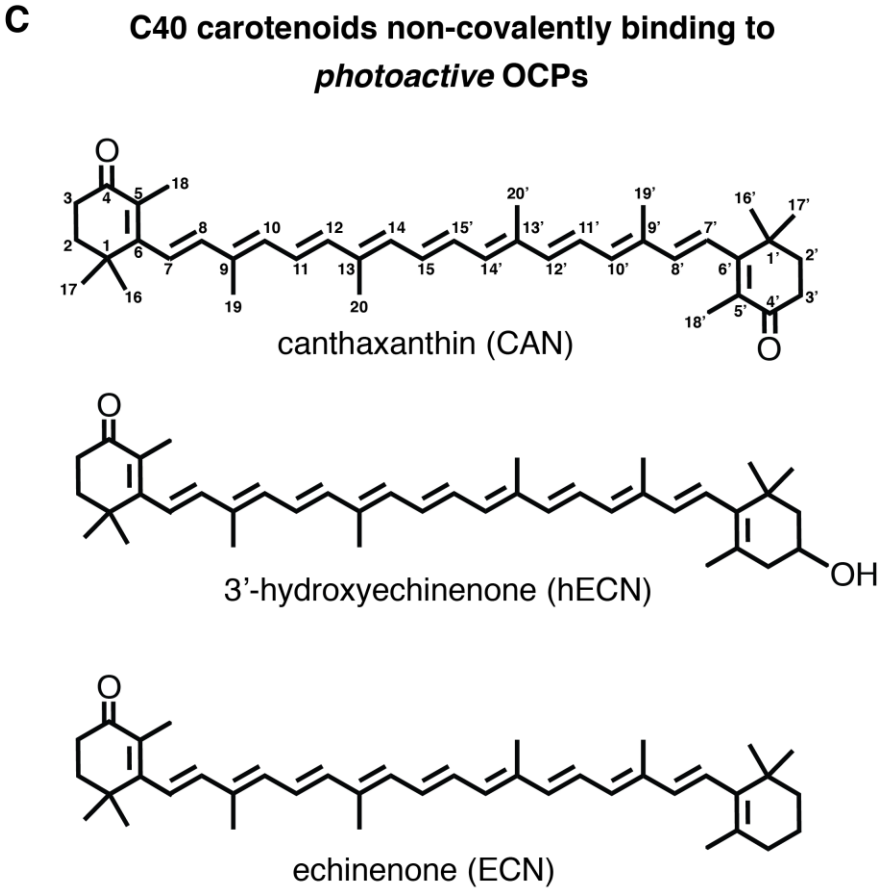

Figure S1. (**C**) Molecular structures of the 4-keto carotenoids (hECN, ECN, and CAN) known to bind to functionally active OCP. Carbon atom numbering is shown for CAN.

Fig. S2

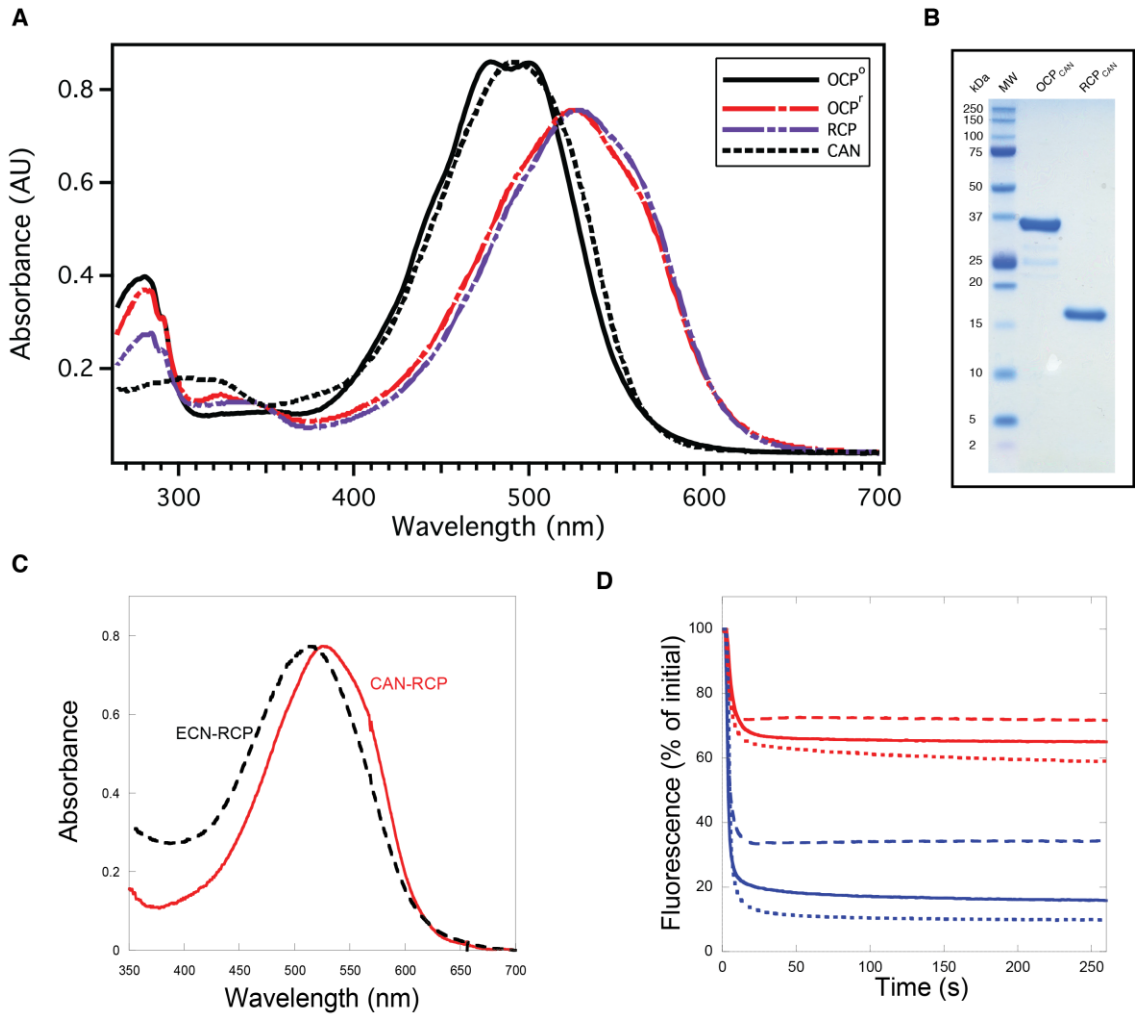

Figure S2. Characterization and comparison of OCP and RCP proteins binding ECN or CAN. (**A**) UV-visible absorption spectrum of purified OCP^O (black), OCP^R (red), and RCP (purple) holoproteins binding CAN. The absorbance spectrum of CAN in DMSO (black, dotted) is also shown. The CAN and RCP spectra were normalized to the OCP^O and OCP^R spectra, respectively. Slight differences in the OCP^R and RCP spectra are attributed to differences in the ECN/CAN binding ratios in the two samples (Table S1). (**B**) SDS-PAGE of OCP_{CAN} and RCP_{CAN} samples used for protein crystallography and XF-MS experiments. (**C**) direct comparison of the UV-Visible spectra of RCP binding ECN (black dashed line) or CAN (red solid line). (**D**) PB fluorescence quenching at 0.8 M phosphate (red traces) or 1.4 M phosphate (blue traces) induced by RCPs binding either ECN or CAN. RCP-CAN (solid lines), RCP-ECN (dashed lines) and RCP from native proteolysis of OCP (dotted lines). RCP-ECN isolated from E. coli cells contained large concentrations of apo-protein (only 1-2% of holoprotein) and reduced solubility (as compared to RCP-CAN) that affected the amplitude of quenching. RCP-CAN also contained about 30-40% of apo-protein that slightly decreased the amplitude of fluorescence quenching relative to the proteolytic RCP.

Fig. S3

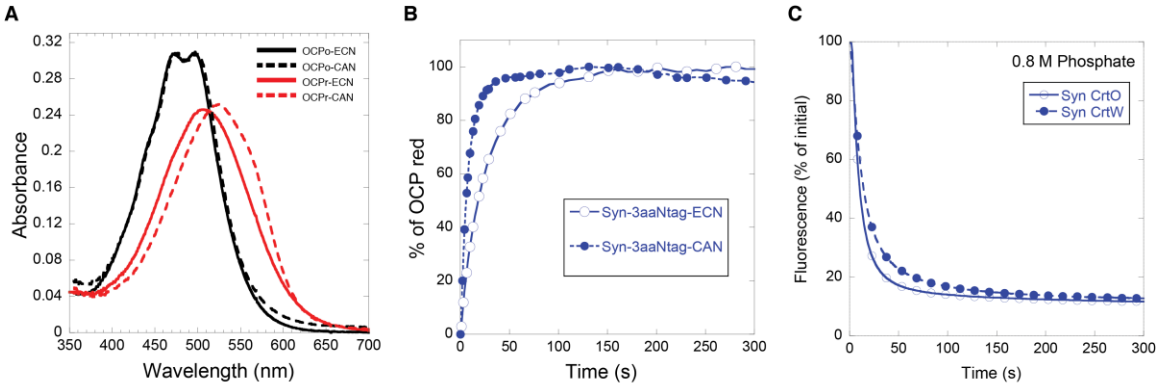

Figure S3. Characterization of *Synechocystis* CAN-OCP and ECN-OCP isolated from *E. coli* cells. (**A**) Absorbance spectra of dark (black) and light (red) forms of CAN-OCP (dashed) and ECN-OCP. The spectrum of the CAN-OCP^R (max 530 nm) is red-shifted compared to ECN-OCP^R (515 nm) and the photoconversion to OCP^R is faster. (**B**) Photoactivity (OCP^R accumulation) of CAN-OCP (closed circles) and ECN-OCP (open circles) during illumination with strong white light. (**C**) PB fluorescence quenching induced by CAN-OCP^R (closed circles) and ECN-OCP^R (open circles) during illumination with strong blue-green light (900 µmol photons m^{-2} s^{-1}) in 0.8 M phosphate at 23°C. The OCP was pre-activated by illumination with strong white light.

Fig. S4

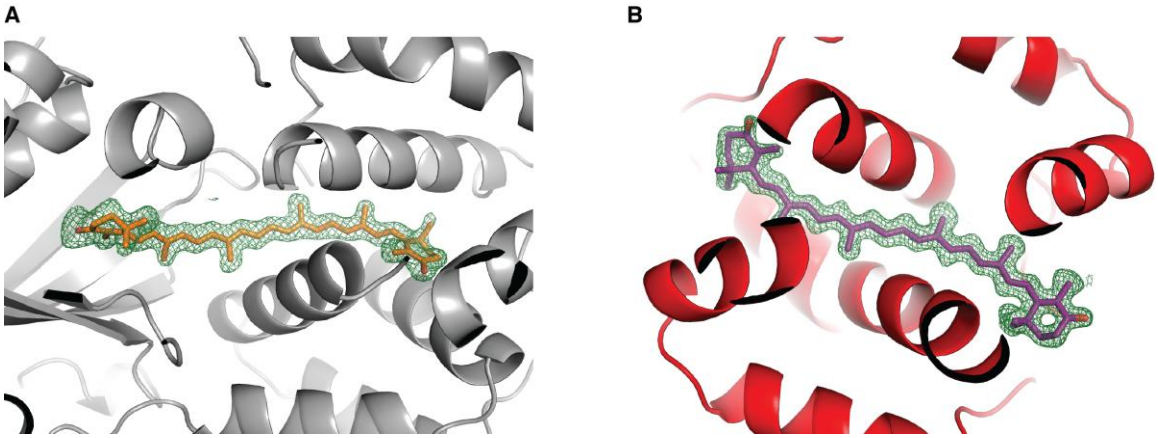

Figure S4. Fo-Fc maps for CAN in OCP and RCP. (**A**), (**B**) Fo-Fc maps from simulated annealing refinement runs without canthaxanthin, contoured at +2.0 sigma around the carotenoid (green mesh). The OCP (**A,** protein in grey ribbon and CAN in orange sticks) and the RCP (**B**, protein in red ribbon CAN in purple sticks) are shown in the same orientation and color scheme as in Fig. 1a but are slabbed to allow a better view of the carotenoid.

Fig. S5

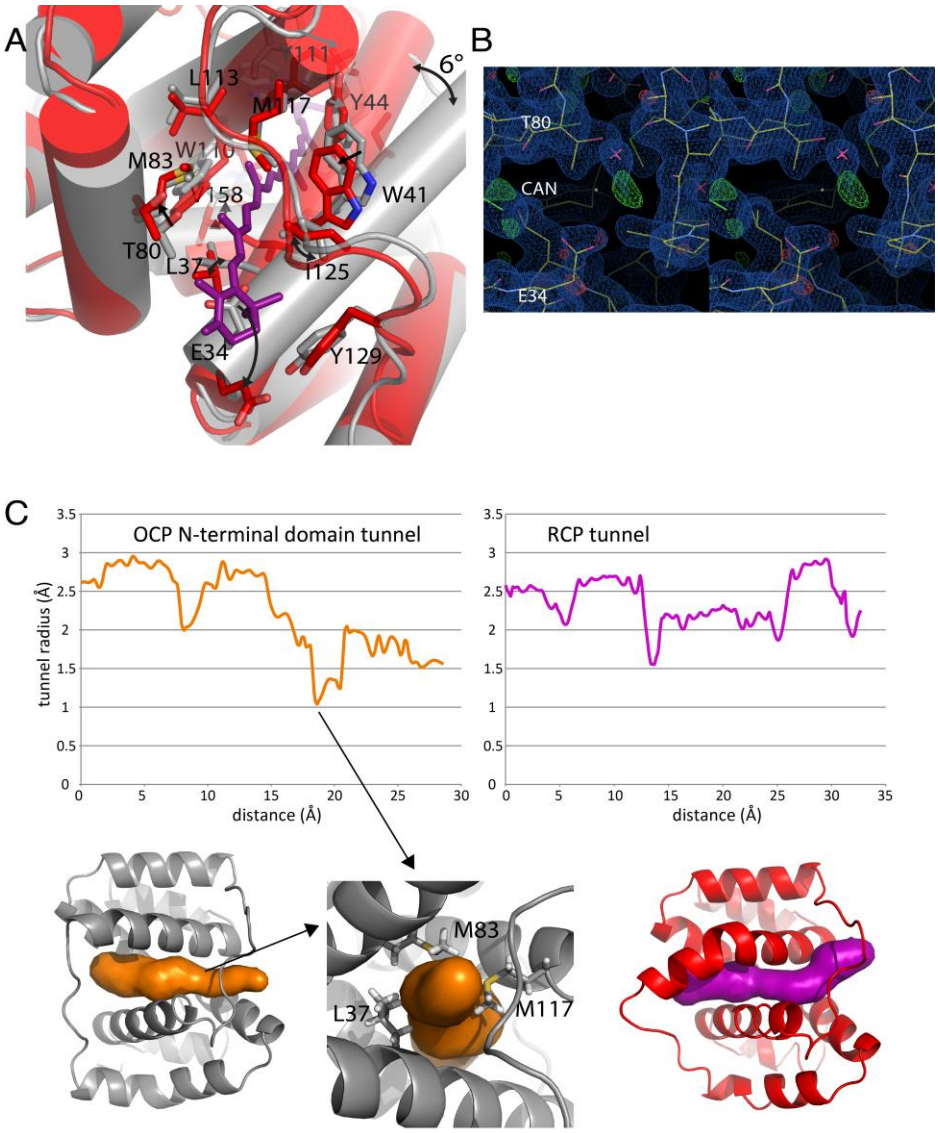

Figure S5. Detailed view of the NTD carotenoid tunnel and analysis of tunnel structure. (A) Alignment of the N-terminal domain of OCP (grey) and RCP (red) with the carotenoid in cpcR configuration (purple) on the site where the carotenoid is translated inwards. Differences between carotenoid interacting sidechains are indicated with single arrows for movement or double arrows indicating a different rotamer. Movements are generally small except for E34 and a 6° rotation of helix C **(B)** Stereo view of the density of the tunnel where the carotenoid is inserted in cpcR (2fofc map in blue, 0.22 e/Å^3, fofc in green(+)/red(-), 0.26e/ Å^3). There is only one ordered water molecule bound on the outside of the tunnel. **(C)** Comparison of the tunnels for both the N-terminal domain of OCP and RCP. Tunnel diameter plots (top) going in the same direction as the surface visualizations below. The smallest diameter in the OCP form is illustrated in detail below as a constriction formed by L37/M83/M117. Tunnel calculations were done using MOLEonline (*47*).

Fig. S5

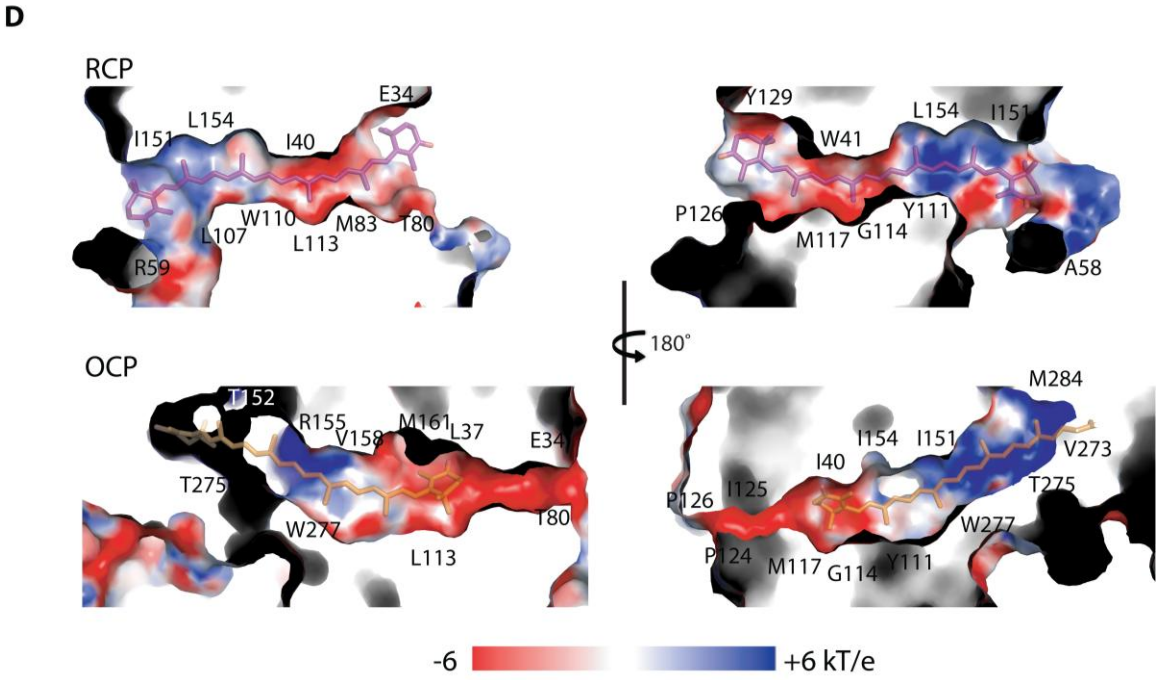

Figure S5. Detailed view of the NTD carotenoid tunnel and analysis of tunnel structure. (D) Electrostatics of the interior surfaces of the N-terminal carotenoid tunnel in RCP and OCP from two slabbed views related by a 180 degree rotation. Positions of residues are indicated to facilitate orientation.

Fig. S6

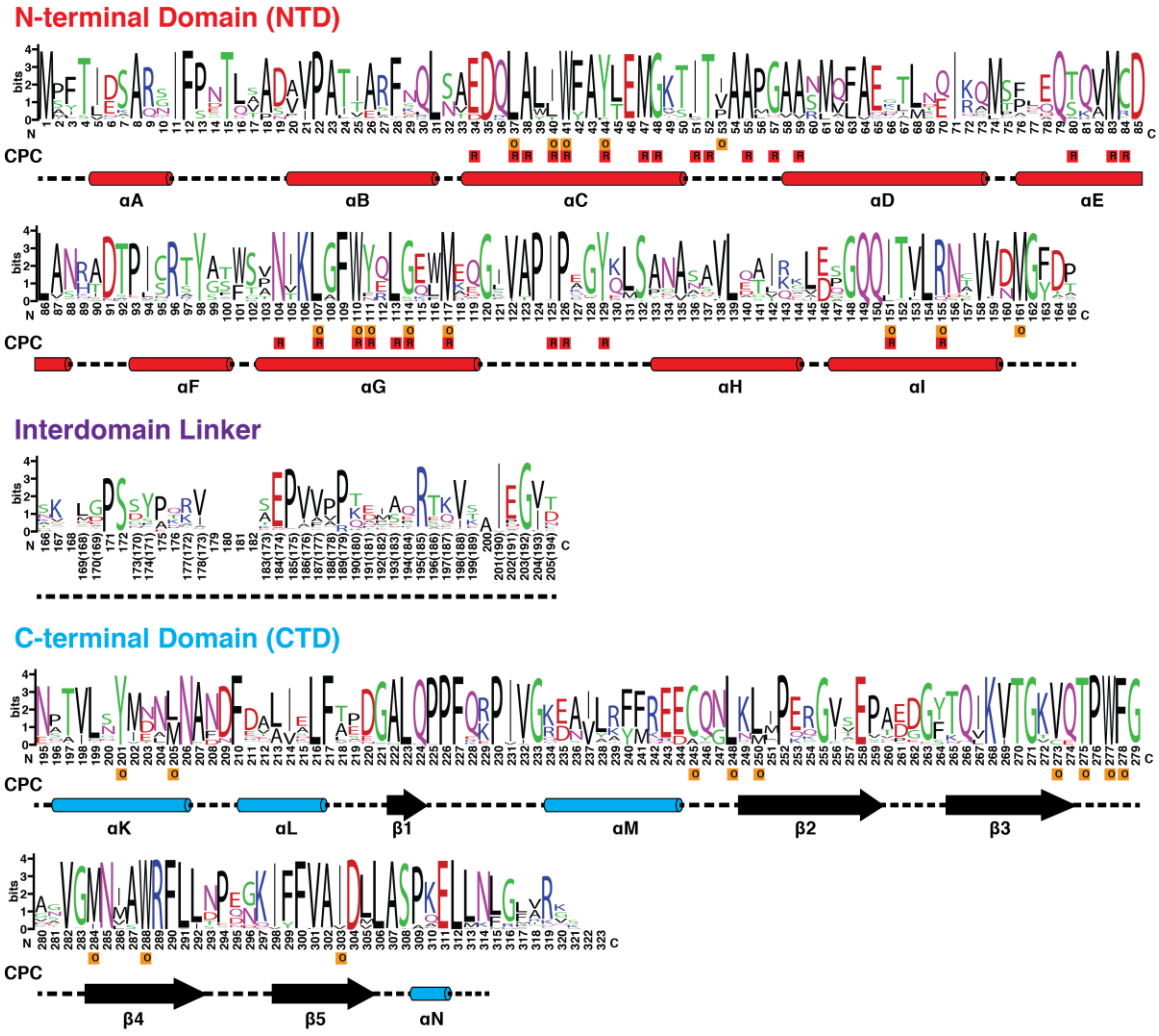

Figure S6. Primary structure sequence logo for full length OCP showing the location of secondary structure and carotenoid binding residues in the OCP and RCP structures. Sequence logos for the NTD, CTD, and interdomain linker are shown separately. Low occupancy insertions (< 1% occurrence) in the NTD and CTD were manually removed to maintain numbering consistency with *Synechocystis* OCP. Low occupancy insertions in the interdomain linker region and C-terminus appear without residue identifiers. Numbers shown in parenthesis in the alignment for the interdomain linker correspond to sequence numbering for *Synechocystis* OCP.

Fig. S7

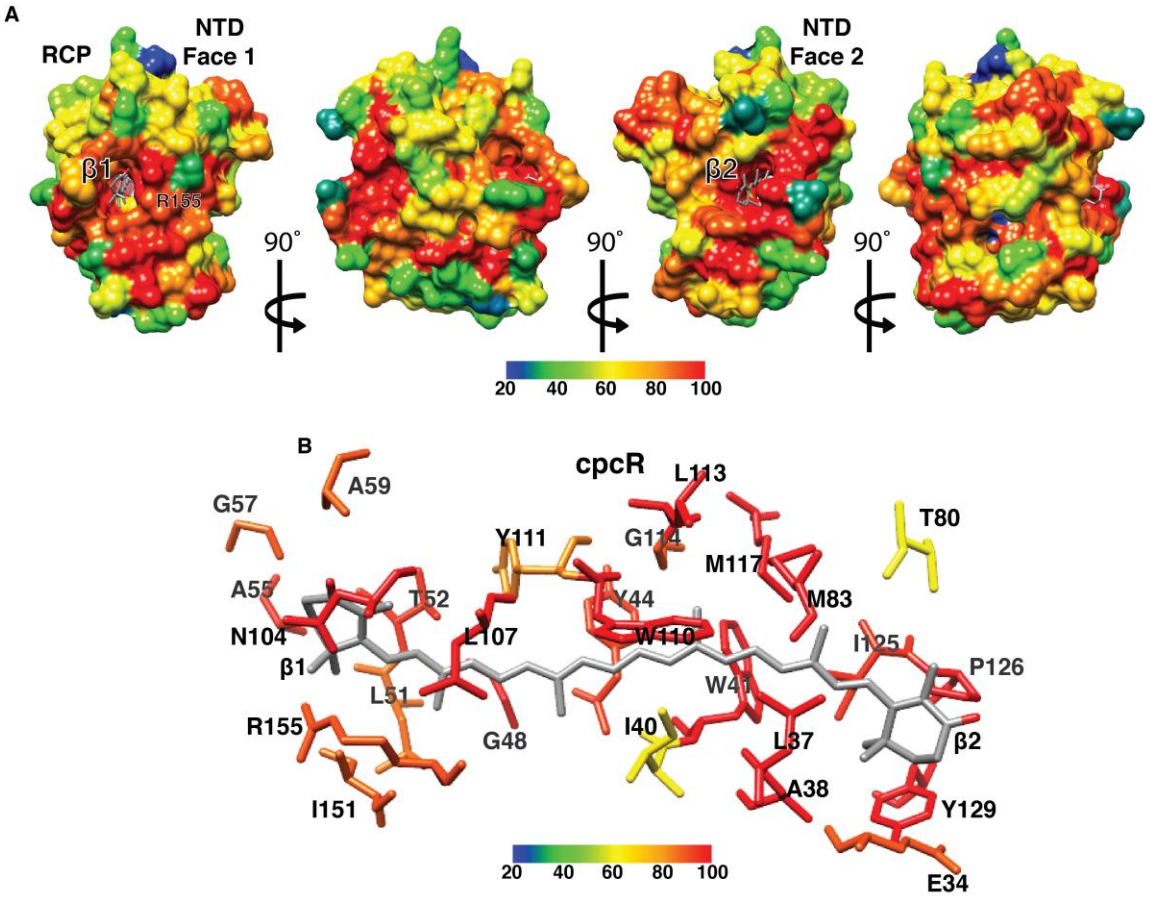

Figure S7. Amino acid sequence conservation mapped onto OCP and RCP structures. (**A**) Sequence conservation of full-length OCP orthologs mapped on the RCP-can structure. Sequence conservation was determined from an alignment of 168 full-length OCP amino acid sequences (see Methods). Maps are colored by percent conservation as indicated by the inset color bar. (**B**) Detailed view of the sequence conservation of CAN binding residues in cpcR (CAN in grey sticks, residues in sticks colored by percent conservation).

Fig. S8

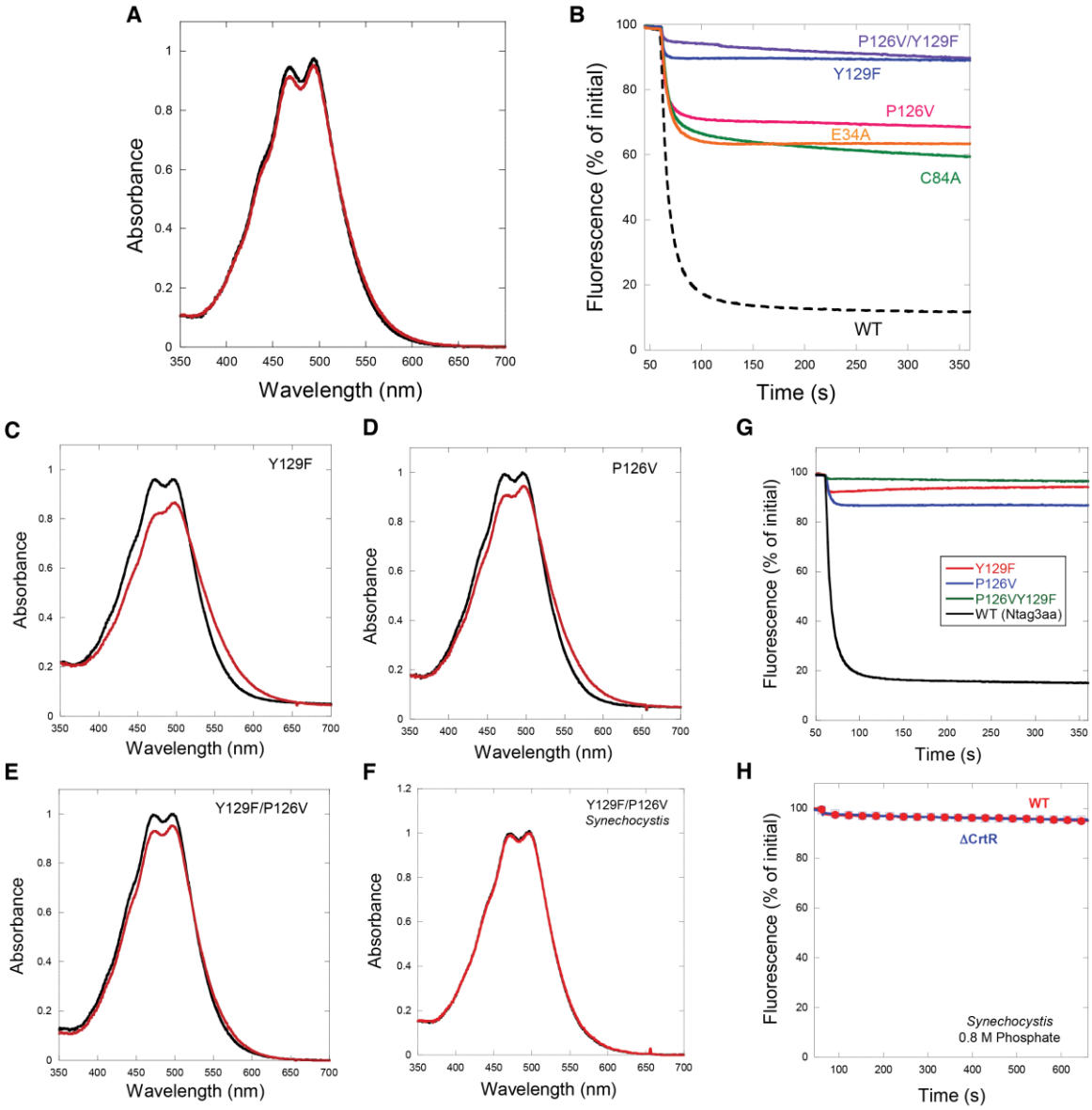

Figure S8. UV-Visible spectra and PB fluorescence quenching of OCPs with mutated cpcR carotenoid binding residues. (**A**) Absorbance spectra of the dark (black) and light (red) forms of the double mutant P126V/Y129F CAN-OCP isolated from *E. coli* cells. (**B**) PB fluorescence quenching induced by WT and mutated CAN-OCPs at 0.8 M phosphate during illumination at 900 µmol photons m^{-2} s^{-1} of blue-green light and 23°C. The OCP were previously illuminated with strong white light to photoactivate them. (**C**)-(**F**) Absorbance spectra of the dark (black) and light (red) forms of single and double mutants of ECN-OCP isolated from *E. coli* or *Synechocystis*. The OCPs were illuminated at 9°C with strong white light during 5 min. (**G**),(**H**) PB fluorescence quenching induced by WT and mutated ECN-OCPs isolated from *E. coli* (**G**) or *Synechocystis* (P126V.Y129F mutant isolated from WT and ΔCrtR background strains) (**H**) in 0.8 M

phosphate, under 900 µmol photons m^{-2} s^{-1} blue-green light and 23°C. The OCPs were pre-illuminated with strong white light before adding to the PBs.

Fig. S9

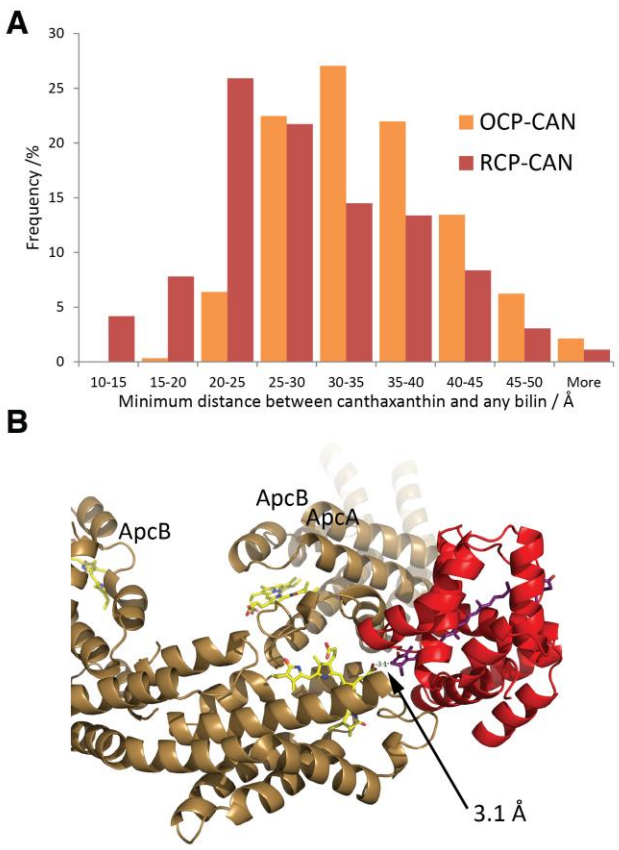

Figure S9. (A) Comparison of the minimal distance between the CAN and any of the bilin chromophores resulting from unconstrained random docking of OCP_{CAN} or RCP_{CAN} to ApcAB. The Y axis indicates how frequent a certain distance range occurs in the 1000 top docking solutions chosen from 25'000 docking runs by highest Rosetta score. **(B)** Result from a constrained docking run indicating that the minimal distance can be a low as 3.1 Å. The situation *in vivo* is likely very different since the exact binding site and mode is not known.

Table S1. Carotenoid content of OCPs and RCPs used in this study. The carotenoid content of purified OCPs and RCPs determined by LC-MS. For proteins expressed in *E. coli*, β-carotene (β-CAR) producing *E. coli* BL21 cells with either pBAD-CrtW or pBAD-CrtO plasmids were used to produce the carbonyl carotenoids CAN and ECN *in vivo* (see Methods). All the OCPs isolated from *E. coli* cells with the pBAD-CrtO plasmid contained around 95% ECN and 5% CAN. The OCPs produced in cells containing the pBAD-CrtW were observed to bind a mixture of ECN and CAN although the cells contained less than 10% of ECN and more than 50% CAN. Certain mutant OCPs (i.e. E34A) were observed to bind ECN and CAN in significantly different amounts as compared to wildtype (WT) OCP, suggesting an importance of cpcR carotenoid-binding residues to the carotenoid binding specificity of OCP. Small amounts of a carotenoid of unknown identity (m/z = 548) were detected for a number of samples, but constituted < 5% of total carotenoid content in all cases. P126V/Y129F OCP mutants expressed in wildtype *Synechocystis* contained moderate amounts of hECN and zeaxanthin (ZEA).

Sample	**Carotenoid content (%)**					
	CAN	ECN	Unknown (m/z = 548)	β-CAR	hECN	ZEA
WT OCPs from *E. coli* (CrtO or CrtW)						
OCP-ECN (CrtO)	5.0	95.0	0	0	0	0
OCP-CAN (CrtW)	43.4	52.6	4.0	0	0	0
Mutant OCPs from *E. coli* (CrtW)						
OCP C84A	54.6	42.1	3.3	0	0	0
OCP E34A	15.9	80.4	3.7	0	0	0
OCP Y129F	31.6	65.2	3.2	0	0	0
OCP P126V	52.5	44.6	2.7	0.2	0	0
OCP P126V/Y129F	45.8	49.3	4.9	0	0	0
WT RCPs from *E. coli* (CrtW)						
RCP-CAN	100	0	0	0	0	0
Mutant OCPs from *Synechocystis*						
P126V/Y129F (wildtype *Synechocystis*)	0	72	0	0	9.5	18.5
P126V/Y129F (ΔCrtR *Synechocystis*)	0.6	99.4	0	0	0	

Table S2. X-ray crystallography data collection and refinement statistics for OCP_{CAN} and RCP_{CAN} data sets. Statistics for the highest-resolution shell are shown in parentheses.

	RCP-CAN	OCP-CAN
Data collection		
Resolution range (Å)	39 - 1.54 (1.60 - 1.54)	37 - 1.90 (1.97 - 1.90)
Space group	P 1 2_1 1	P 3_2 2 1
Unit cell dimensions	51.3 64.1 53.6 Å 90 115 90 °	82.9 82.9 87.2 Å 90 90 120 °
Total reflections	91995 (8763)	55545 (5518)
Unique reflections	46069 (4431)	27757 (2759)
Multiplicity	7.2 (6.9)	20.7 (20.3)
Completeness (%)	99.6 (96.3)	99.9 (99.4)
Mean I/sigma(I)	13.8 (2.5)	23.9 (2.1)
Wilson B-factor	16.3	28.9
R-merge	0.025 (0.32)	0.017 (0.36)
R-meas	0.035	0.023
$CC^{1/2}$	0.999 (0.799)	1 (0.839)
CC*	1 (0.943)	1 (0.955)
Refinement		
Number of reflections	46063	27746
Number of reflections used for R-free	1998	2008
R-work (%)	14.74 (25.95)	18.09 (43.46)
R-free (%)	15.99 (29.45)	20.76 (43.19)
Number of non-hydrogen atoms	2644	2694
macromolecules	2196	2410
ligands	84	48
solvent	364	236
Protein residues	282	315
RMS (bonds, Å)	0.007	0.006
RMS (angles, °)	1.04	0.90
Ramachandran favored (%)	99	99
Ramachandran allowed (%)	1	1
Ramachandran outliers (%)	0	0
Clashscore	0.67	1.64
Average B-factor ($Å^2$)	21.5	33.7
macromolecules ($Å^2$)	19.3	33.3
ligands ($Å^2$)	21.2	24.1
solvent ($Å^2$)	35.0	39.8

Table S3. Comparison of canthaxanthin dihedral angles observed in OCP and RCP structures. Dihedral angles were measured using atomic PDB coordinates for CAN carbon atoms. Dihedral angles for 3'-hECN binding (PDB ID: 1M98) and ECN binding (PDB ID: 3MG1) OCPs are also included for comparison.

Dihedral	**RCP_{CAN} (Chain A)**	**RCP_{CAN} (Chain B)**	**OCP_{CAN}**	**Synechocystis OCP (3MG1 - Chain A)**	**Synechocystis OCP (3MG1 - Chain B)**	**Arthrospira OCP (1M98 - Chain A)**	**Arthrospira OCP (1M98 - Chain B)**
C5-C6-C7-C8 (β1 ring)	-63.5	39.8	116.3	146.4	148.6	118.5	131.9
C6-C7-C8-C9	177.9	179.0	175.4	171.0	172.2	172.8	174.7
C7-C8-C9-C10	-146.5	-170.0	-155.3	-179.5	179.5	-163.7	-176.8
C8-C9-C10-C11	177.6	178.0	175.8	169.3	170.9	177.9	171.1
C9-C10-C11-C12	-173.5	177.2	178.8	173.2	173.5	165.2	173.6
C10-C11-C12-C13	176.1	176.8	174.4	169.6	171.4	175.4	175.5
C11-C12-C13-C14	-178.9	-172.8	167.8	172.8	178.0	177.5	175.9
C12-C13-C14-C15	171.1	175.8	173.0	-177.3	-178.8	171.0	170.0
C13-C14-C15-C16	177.1	173.9	-171.4	-175.2	179.8	-175.7	171.5
C14-C15-C15'-C14'	178.3	176.0	172.7	168.7	167.7	170.7	171.4
C15-C15'-C14'-C13'	-176.9	-175.8	169.8	178.9	178.0	179.6	-168.2
C15'-C14'-C13'-C12'	-179.1	178.4	173.0	170.9	170.4	172.8	169.8
C14'-C13'-C12'-C11'	-175.0	-178.6	-153.3	-172.4	-171.5	-161.6	171.4
C13'-C12'-C11'-C10'	-178.2	-179.7	173.1	171.4	171.0	174.8	170.9
C12'-C11'-C10'-C9'	179.6	179.7	171.9	-177.3	-178.1	170.3	-158.8
C11'-C10'-C9'-C8'	-179.9	178.5	175.2	174.2	174.6	174.0	-179.7
C10'-C9'-C8'-C7'	-179.5	168.7	-160.3	-180.0	-179.4	-170.2	174.9
C9'-C8'-C7'-C6'	178.8	177.5	177.6	177.2	176.8	177.3	178.6
C8'-C7'-C6'-C5' (β2 ring)	163.3	-146.1	-72.1	-52.7	-52.8	-66.0	-51.9

Table S4.

(A) Canthaxanthin binding residues observed in the OCP carotenoid-binding pocket. The shortest distance between CAN and a particular residue is listed, along with the specific atoms (in PDB atom numbering) that define the distance of closest approach. Sequence conservation is based on the alignment described in the Methods. Shared residues in cpcO and cpcR are listed in bold.

cpcO - CAN Binding Residues in OCP				
Residue	**Residue Atom**	**CAN Atom**	**Distance (Å)**	**Sequence Conservation**
Leu37	**CD2**	**O02**	**3.34**	**L (1.00)**
Ile40	**CG2**	**C16**	**3.41**	**I (0.649), L(0.280), T(0.071)**
Trp41	**N**	**C06**	**3.66**	**W (1.00)**
Tyr44	**CG**	**C14**	**3.26**	**Y(0.958), F(0.042)**
Ile53	CG2	C40	3.96	V(0.369), I(0.369), P(0.226), R(0.018), A(0.018)
Leu107	**CD2**	**C36**	**3.78**	**L(1.00)**
Trp110	**CD2**	**C22**	**3.61**	**W(1.00)**
Tyr111	**N**	**C28**	**3.61**	**Y(0.851), N(0.071), F(0.071),W(0.006)**
Gly114	**CA**	**C13**	**3.56**	**G(0.917), S(0.060), A(0.024)**
Met117	**SD**	**C13**	**3.81**	**M(1.00)**
Ille151	**O**	**C41**	**3.64**	**I(0.899), L(0.101)**
Thr152	OG1	C39	3.51	T(0.958), S(0.030), Q(0.012)
Arg155	**CD**	**C35**	**3.71**	**R(0.911), Q(0.083), H(0.006)**
Val158	CG2	C22	3.66	V(0.994), I(0.006)
Met161	CE	O02	3.66	M(1.00)
Tyr201	OH	O01	2.56	Y(1.00)
Leu205	CD2	O01	3.61	L(0.565), M(0.435)
Cys245	SG	C12	3.54	C(0.887), A(0.107), G(0.006)
Leu248	CD1	C07	3.95	L(1.00)
Leu250	CD2	O01	3.66	L(0.821), M(0.167), I(0.012)
Val273	CG2	C21	3.56	V(0.905), C(0.095)
Thr275	CB	C33	3.79	T(0.982), S(0.018)
Trp277	CD2	C40	3.73	W(1.00)
Phe278	CE2	C42	3.91	F(0.982), A(0.012), V(0.006)
Met284	CE	C31	3.57	M(0.899), I(0.095), L(0.006)
Trp288	NE1	O01	2.87	W(1.00)
Ile303	CG1	O01	3.66	I(0.935), V(0.065)

Table S4.

(B) Canthaxanthin binding residues observed in the RCP carotenoid-binding pocket. Distances and atom numbering are the same as in (S4.A.).

cpcR - CAN Binding Residues in RCP				
Residue	**Residue Atom**	**CAN Atom**	**Distance (Å)**	**Sequence Conservation**
Glu34	O (A), O (B)	C11 (A), C11 (B)	3.43 (A), 3.61 (B)	E(0.899), D(0.101)
Leu37	**CG (A), CD2 (B)**	**C29 (A), C23 (B)**	**3.43 (A), 3.58 (B)**	**L(1.00)**
Ala38	N (A), N (B)	C11 (A), C11 (B)	3.97 (A), 3.78 (B)	A(0.994), G(0.006)
Ile40	**O (A), O (B)**	**C42 (A), C42 (B)**	**3.41 (A), 3.30 (B)**	**I (0.649), L(0.280), T(0.071)**
Trp41	**CB (A), CB (B)**	**C33 (A), C33 (B)**	**3.68 (A), 3.57 (B)**	**W (1.00)**
Tyr44	**CB (A), CB (B)**	**C40 (A), C42 (B)**	**3.56 (A), 3.51 (B)**	**Y(0.958), F(0.042)**
Met47*	SD(A)	C32(A)	3.75(A)	M(0.964), T(0.012), L(0.012), I(0.012)
Gly48*	CA (B)	C32 (B)	3.91 (B)	G(0.994), A(0.006)
Leu51*	O (B)	C14 (B)	3.85 (B)	I(0.887), L(0.077), V(0.036)
Thr52*	OG1 (B)	C24 (B)	3.55 (B)	T(0.970), S(0.024), I(0.006)
Ala55*	CB (B)	C06 (B)	2.72 (B)	A(0.988), T(0.006), S(0.006)
Gly57*	O (B)	C06 (B)	3.64 (B)	G(0.911), D(0.030), Q(0.024), S(0.018), A(0.012), E(0.006)
Ala59*	CB (B)	O02 (B)	3.18 (B)	A(0.899), V(0.077), T(0.024)
Thr80	CG2 (A), CG2 (B)	C21 (A), C21 (B)	3.16 (A), 3.44 (B)	T(0.607), S(0.321), A(0.042), E(0.018), M(0.006), F(0.006)
Met83	CE (A), CE (B)	C27 (A), C27 (B)	3.46 (A), 3.54 (B)	M(1.00)
Cys84*	SG.A (A)	C21 (A)	3.88 (A)	C(0.810), R(0.113), Y(0.024), F(0.024), T(0.012), V(0.006), I (0.006), H(0.006)
Asn104	OD1 (A), CB (B)	C13 (A), O02 (B)	3.28 (A), 3.49 (B)	N(1.00)
Leu107	**O (A), CA (B)**	**C30 (A), C32 (B)**	**3.88 (A), 3.84 (B)**	**L(1.00)**
Trp110	**O (A), O (B)**	**C41 (A), C41 (B)**	**3.43 (A), 3.40 (B)**	**W(1.00)**
Tyr111	**N (A), N (B)**	**C38 (A), C38 (B)**	**3.83 (A), 3.85 (B)**	**Y(0.851), N(0.071), F(0.071),W(0.006)**
Leu113	CB (A), CB (B)	C39 (A), C39 (B)	3.92 (A), 3.94 (B)	L(1.00)
Gly114	**N (A), N (B)**	**C39 (A), C39 (B)**	**3.77 (A), 3.68 (B)**	**G(0.917), S(0.060), A(0.024)**
Met117	**SD (A), SD (B)**	**C39 (A), C39 (B)**	**3.64 (A), 3.68 (B)**	**M(1.00)**
Ile125	CG2 (A), CG2 (B)	C25 (A), C23 (B)	3.77 (A), 3.80 (B)	I(0.899), L(0.101)
Pro126	CD (A), CD (B)	C07 (A), C07 (B)	3.65 (A), 3.90 (B)	P(1.00)
Tyr129	CE1 (A), CE1 (B)	C05 (A), C05 (B)	3.44 (A), 3.47 (B)	Y(1.00)
Ile151	**CG1 (A), CD1 (B)**	**C28 (A), C14 (B)**	**3.95 (A), 3.60 (B)**	**I(0.899), L(0.101)**
Arg155	**NH2 (A), NH2 (B)**	**C14 (A), C13 (B)**	**3.86 (A), 3.82 (B)**	**R(0.911), Q(0.083), H(0.006)**

Table S5. Peptides and specific modification sites detected by XF-MS and the ratio(s) of hydroxyl radical reactivity. Detected peptides, modification sites, and their corresponding hydroxyl radical reactivity ratios (R) are listed for OCP_{CAN}, RCP_{CAN}, and RCP_{ECN} protein samples.

Seq. No.[a]	Peptide Sequence[c]	Site of modification[d]	Ratio "R" of hydroxyl radical reactivity[e]		
			$k_{OCP}^{R} / k_{OCP}^{O}$	$k_{RCP-CAN} / k_{OCP}^{O}$	$k_{RCP-ECN} / {}^{k}k_{OCP}^{O}$
2-9	PFTIDSAR	P1, F2 (+16 Da)[g]	-[i]	-	-
		A8, R9 (+16 Da)	-	-	-
10-27	GIFPNTLAADVVPATIAR	Residues 13 to 22 (+16 Da)	1.37 ± 0.15	-	1.10 ± 0.24
28-49	FSQLNAEDQLALIWFAYL EMGK	W41 (+48 Da)	0.35 ± 0.05	0.55 ± 0.05	0.11 ± 0.03
		W41, F42, Y44, M47 (+16 Da)	0.45 ± 0.05	0.61 ± 0.06	0.15 ± 0.03
		M47 (+16 Da)	0.79 ± 0.08	0.87 ± 0.09	0.33 ± 0.04
50-69	TLTIAAPGAASMQLAENA LK	P56 (+16 Da)	0.71 ± 0.14	0.73 ± 0.14	0.37 ± 0.08
		M61 (+16 Da)	1.45 ± 0.19	0.89 ± 0.14	0.51 ± 0.08
70-89	EIQAMGPLQQTQAMCDL ANR	M74P76M83 (+16 Da)	1.10 ± 0.24	0.82 ± 0.20	0.31 ± 0.04
90-96	ADTPLCR	P94 (+16 Da)	0.79 ± 0.12	0.79 ± 0.12	0.34 ± 0.08
97-106	TYASWSPNIK	Y98W101P103 (+16 and + 32 Da)	2.84 ± 0.63	2.72 ± 0.61	1.00 ± 0.16
107-112	LGFWY	F109W110Y111 (+16 and + 32 Da)	0.98 ± 0.26	1.64 ± 0.35	0.74 ± 0.13
113-155	LGELMEQGFVAPIPAGYQ LSANANAVLATIQGLESG QQITVLR	M117 (+16 Da)	0.83 ± 0.12	1.22 ± 0.15	0.59 ± 0.10
119-146[b]	QGFVAPIPAGYQLSANAN AVLATIQGLE	Residues 121-126 (+16 Da)[h]	0.73 ±0.18	1.10 ± 0.23	0.40 ± 0.05
147-160[b]	SGQQITVLRNAVVD	R155, N156 (+16 Da)	10.25 ± 3.54	17.25 ± 5.76	4.74 ± 0.62
156-167	NAVVDMGFTAGK	M161 (+16 Da)	1.27 ± 0.07	-	0.25 ± 0.03
		F163 (+16 Da)	0.58 ± 0.20	-	0.39 ± 0.06
		K167 (+16 Da)	0.78 ± 0.16	-	0.55 ± 0.12
172-185	IAEPVVPPQDTASR	P175P178P179R185 (+16 Da)	0.67 ± 0.15	--[j]	--
192-215[b]	GVTNATVLNYMDNLNAN DFDTLIE	Residues 119 to 215 (+16 Da)[h]	1.11 ± 0.21	--	--
221-235[b]	GALQPPFQRPIVGKE	Residues 226 to 231 (+16 Da)[h]	1.47 ± 0.27	--	--
235-239	ENVLR	R239 (+16 Da)	0.76 ± 0.05	--	--
243-249	EECQNLK	No modification[f]	-	--	--
250-254	LIPER	P252 (+16 Da)	0.53 ± 0.06	--	--
255-268	GVTEPAEDGFTQIK	P259, F264, K268 (+16 Da)	0.91 ± 0.20	--	--
273-289	VQTPWFGGNVGMNIAWR	P276, W277, F278 (+32 Da)	3.38 ± 0.38	--	--
		M284 (+16 Da)	2.88 ± 0.32	--	--
290-297	FLLNPEGK	F190 (+16 Da)	1.67 ± 0.15	--	--
		L291, L292 (+16 Da)	0.92 ± 0.06	--	--
		P294 (+16 Da)	0.97 ± 0.10	--	--
298-310	IFFVAIDLLASPK	I298, F299 (+16 Da)	1.89 ± 0.33	--	--
		V301, A302, I303 (+16 Da)	1.86 ± 0.30	--	--
		P309, K310 (+16 Da)	0.75 ± 0.15	--	--

[a] 94 % sequence coverage was obtained from the bottom up LC-ESI-MS analysis of OCPO, OCPR, RCP-CAN, and RCP-ECN using trypsin and [b] Glu c digestions.
[c] sequences of digested fragments identified by mass spectrometry analysis described in experimental procedures
[d] positions of modified residues identified mass spectrometry analysis described in experimental procedures. Multiple residues are indicated by sequence number
[e] rate constants were estimated by employing a non-linear fit of hydroxyl radical modification data to a first order decay as described in experimental procedures. R is a quantitative measure of the change in the solvent accessibility changes. Reported errors were determined from the maximum and minimum values of R calculated from the non-regression fit parameter (k) and its standard error obtained from a single dose response within 95% confidence interval.
[f] no modification was detected
[g] mass shift due to side chain modification is show within the parenthesis
[i] no data available either due to missing sequence in the contrast or no modification
[j] comparison not done due to the absence of CTD in RCPs
[k] rate constant measured from OCP^{O}-ECN sample

Table S6. Sequences of primers used in this study. Listed primers include those used for construction of 6x-His tagged RCPs (**A, B**) and those used for site-directed mutagenesis (**C**) as described in the Methods section

A.Primers used for construction of RCP 1-165 His6-tagged C-terminal plasmid for expression in *E.coli*	
RCP-Syn-1-165-Ctag-F	CATCATCATCATCATCATTAGAATAACTCCCTTCAGAGTTTTGTCT
RCP-Syn-1-165-Ctag-R	ATGATGATGATGATGATGAGCGGTGAAGCCCATGTCCAC
B. Primer used for construction of RCP 20-165 His6-tagged C-terminal plasmid for expression in *E.coli*	
RCP-Syn-20-165-Ctag-F	TTAATAAGGAGATATACCATGGTACCCGCTACCATCGCCCGT
RCP-Syn-20-165-Ctag-R	CATGGTATATCTCCTTATTAAAGTTAAACAAAATTATTTCTA
C. Site-directed mutagenesis primers	
P126V - F	GCCCCAATTGTCGCTGGTTACCAACTTTCTGCC
P126V - R	GGCAGAAAGTTGGTAACCAGCGACAATTGGGGC
P126A - F	CCAATTGCCGCTGGTTACCAACTTTCTGCC
P126A - R	GGCAGAAAGTTGGTAACCAGCGGCAATTGG
Y129F - F	GCCCCAATTCCCGCTGGTTTCCAACTTTCTGCC
Y129F -R	GGCAGAAAGTTGGAAACCAGCGGGAATTGGGGC
P126V/Y129F - F	GCCCCAATTGTCGCTGGTTTCCAACTTTCTGCC
P126V/Y129F - R	GGCAGAAAGTTGGAAACCAGCGACAATTGGGGC
E34A - F	CTCAATGCCGCAGATCAATTGGCTCTGATTTGGTTTGCTTACC
E34A - R	AATCAGAGCCAATTGATCTGCGGCATTGAGTTGGCTAAAACG
C84A - F	CAAACCCGGGCCATGGCTGACTTGGC
C84A - R	GCCAAGTCAGCCATGGCCCGGGTTTGG

References

1. R. Croce, H. van Amerongen, Natural strategies for photosynthetic light harvesting. *Nat. Chem. Biol.* **10**, 492–501 (2014). Medline doi:10.1038/nchembio.1555

2. P. Horton, A. V. Ruban, R. G. Walters, Regulation of light harvesting in green plants (indication by nonphotochemical quenching of chlorophyll fluorescence). *Plant Physiol.* **106**, 415–420 (1994). Medline

3. D. Kirilovsky, Photoprotection in cyanobacteria: The orange carotenoid protein (OCP)-related non-photochemical-quenching mechanism. *Photosynth. Res.* **93**, 7–16 (2007). Medline doi:10.1007/s11120-007-9168-y

4. K. K. Niyogi, T. B. Truong, Evolution of flexible non-photochemical quenching mechanisms that regulate light harvesting in oxygenic photosynthesis. *Curr. Opin. Plant Biol.* **16**, 307–314 (2013). Medline doi:10.1016/j.pbi.2013.03.011

5. A. A. Pascal, Z. Liu, K. Broess, B. van Oort, H. van Amerongen, C. Wang, P. Horton, B. Robert, W. Chang, A. Ruban, Molecular basis of photoprotection and control of photosynthetic light-harvesting. *Nature* **436**, 134–137 (2005). Medline doi:10.1038/nature03795

6. H. Staleva, J. Komenda, M. K. Shukla, V. Šlouf, R. Kaňa, T. Polívka, R. Sobotka, Mechanism of photoprotection in the cyanobacterial ancestor of plant antenna proteins. *Nat. Chem. Biol.* **11**, 287–291 (2015). Medline doi:10.1038/nchembio.1755

7. H. A. Frank, A. Cua, V. Chynwat, A. Young, D. Gosztola, M. R. Wasielewski, Photophysics of the carotenoids associated with the xanthophyll cycle in photosynthesis. *Photosynth. Res.* **41**, 389–395 (1994). Medline doi:10.1007/BF02183041

8. T. K. Ahn, T. J. Avenson, M. Ballottari, Y. C. Cheng, K. K. Niyogi, R. Bassi, G. R. Fleming, Architecture of a charge-transfer state regulating light harvesting in a plant antenna protein. *Science* **320**, 794–797 (2008). Medline

9. A. V. Ruban, R. Berera, C. Ilioaia, I. H. van Stokkum, J. T. Kennis, A. A. Pascal, H. van Amerongen, B. Robert, P. Horton, R. van Grondelle, Identification of a mechanism of

photoprotective energy dissipation in higher plants. *Nature* **450**, 575–578 (2007). Medline doi:10.1038/nature06262

10. S. Bode, C. C. Quentmeier, P. N. Liao, N. Hafi, T. Barros, L. Wilk, F. Bittner, P. J. Walla, On the regulation of photosynthesis by excitonic interactions between carotenoids and chlorophylls. *Proc. Natl. Acad. Sci. U.S.A.* **106**, 12311–12316 (2009). Medline doi:10.1073/pnas.0903536106

11. P. J. Walla, C.-P. Holleboom, G. R. Fleming, in *Non-Photochemical Quenching and Energy Dissipation in Plants, Algae and Cyanobacteria*, B. Demmig-Adams, G. Garab, W. A. III, Govindjee, Eds. (Springer, Amsterdam, 2014), pp. 229–243.

12. A. Wilson, C. Punginelli, A. Gall, C. Bonetti, M. Alexandre, J. M. Routaboul, C. A. Kerfeld, R. van Grondelle, B. Robert, J. T. Kennis, D. Kirilovsky, A photoactive carotenoid protein acting as light intensity sensor. *Proc. Natl. Acad. Sci. U.S.A.* **105**, 12075–12080 (2008). Medline doi:10.1073/pnas.0804636105

13. M. Gwizdala, A. Wilson, D. Kirilovsky, In vitro reconstitution of the cyanobacterial photoprotective mechanism mediated by the Orange Carotenoid Protein in *Synechocystis* PCC 6803. *Plant Cell* **23**, 2631–2643 (2011). Medline doi:10.1105/tpc.111.086884

14. C. A. Kerfeld, M. R. Sawaya, V. Brahmandam, D. Cascio, K. K. Ho, C. C. Trevithick-Sutton, D. W. Krogmann, T. O. Yeates, The crystal structure of a cyanobacterial water-soluble carotenoid binding protein. *Structure* **11**, 55–65 (2003). Medline doi:10.1016/S0969-2126(02)00936-X

15. C. Punginelli, A. Wilson, J.-M. Routaboul, D. Kirilovsky, Influence of zeaxanthin and echinenone binding on the activity of the orange carotenoid protein. *Biochim. Biophys. Acta Bioenerg.* **1787**, 280–288 (2009). Medline doi:10.1016/j.bbabio.2009.01.011

16. R. L. Leverenz, D. Jallet, M. D. Li, R. A. Mathies, D. Kirilovsky, C. A. Kerfeld, Structural and functional modularity of the orange carotenoid protein: Distinct roles for the N- and C-terminal domains in cyanobacterial photoprotection. *Plant Cell* **26**, 426–437 (2014). Medline doi:10.1105/tpc.113.118588

17. H. Liu, H. Zhang, D. King, N. R. Wolf, M. Prado, M. L. Gross, R. E. Blankenship, Mass spectrometry footprinting reveals the structural rearrangements of cyanobacterial orange

carotenoid protein upon light activation. *Biochim. Biophys. Acta Bioenerg.* **1837**, 1955–1963 (2014). Medline doi:10.1016/j.bbabio.2014.09.004

18. M. Sutter, A. Wilson, R. L. Leverenz, R. Lopez-Igual, A. Thurotte, A. E. Salmeen, D. Kirilovsky, C. A. Kerfeld, Crystal structure of the FRP and identification of the active site for modulation of OCP-mediated photoprotection in cyanobacteria. *Proc. Natl. Acad. Sci. U.S.A.* **110**, 10022–10027 (2013). Medline doi:10.1073/pnas.1303673110

19. A. Wilson, J. N. Kinney, P. H. Zwart, C. Punginelli, S. D'Haene, F. Perreau, M. G. Klein, D. Kirilovsky, C. A. Kerfeld, Structural determinants underlying photoprotection in the photoactive orange carotenoid protein of cyanobacteria. *J. Biol. Chem.* **285**, 18364–18375 (2010). Medline doi:10.1074/jbc.M110.115709

20. R. Berera, I. H. van Stokkum, M. Gwizdala, A. Wilson, D. Kirilovsky, R. van Grondelle, The photophysics of the orange carotenoid protein, a light-powered molecular switch. *J. Phys. Chem. B* **116**, 2568–2574 (2012). Medline doi:10.1021/jp2108329

21. S. Gupta, R. D'Mello, M. R. Chance, Structure and dynamics of protein waters revealed by radiolysis and mass spectrometry. *Proc. Natl. Acad. Sci. U.S.A.* **109**, 14882–14887 (2012). Medline doi:10.1073/pnas.1209060109

22. A. Wilson, M. Gwizdala, A. Mezzetti, M. Alexandre, C. A. Kerfeld, D. Kirilovsky, The essential role of the N-terminal domain of the orange carotenoid protein in cyanobacterial photoprotection: Importance of a positive charge for phycobilisome binding. *Plant Cell* **24**, 1972–1983 (2012). Medline doi:10.1105/tpc.112.096909

23. C. A. Kerfeld, M. Alexandre, D. Kirilovsky, in *Carotenoids: Physical, Chemical and Biological Functions and Properties*, J.T. Landrum, Ed. (CRC Press, Boca Raton, FL, 2009), pp. 3–17.

24. U. K. Genick, G. E. Borgstahl, K. Ng, Z. Ren, C. Pradervand, P. M. Burke, V. Srajer, T. Y. Teng, W. Schildkamp, D. E. McRee, K. Moffat, E. D. Getzoff, Structure of a protein photocycle intermediate by millisecond time-resolved crystallography. *Science* **275**, 1471–1475 (1997). Medline doi:10.1126/science.275.5305.1471

25. J. D. King, H. Liu, G. He, G. S. Orf, R. E. Blankenship, Chemical activation of the cyanobacterial orange carotenoid protein. *FEBS Lett.* **588**, 4561–4565 (2014). Medline doi:10.1016/j.febslet.2014.10.024

26. G. D. Scholes, K. P. Ghiggino, Electronic interactions and interchromophore excitation transfer. *J. Phys. Chem.* **98**, 4580–4590 (1994). doi:10.1021/j100068a017

27. D. Jallet, M. Gwizdala, D. Kirilovsky, ApcD, ApcF and ApcE are not required for the Orange Carotenoid Protein related phycobilisome fluorescence quenching in the cyanobacterium *Synechocystis* PCC 6803. *Biochim. Biophys. Acta Bioenerg.* **1817**, 1418–1427 (2012). doi:10.1016/j.bbabio.2011.11.020

28. D. Jallet, A. Thurotte, R. L. Leverenz, F. Perreau, C. A. Kerfeld, D. Kirilovsky, Specificity of the cyanobacterial orange carotenoid protein: Influences of orange carotenoid protein and phycobilisome structures. *Plant Physiol.* **164**, 790–804 (2014). Medline doi:10.1104/pp.113.229997

29. H. Zhang, H. Liu, D. M. Niedzwiedzki, M. Prado, J. Jiang, M. L. Gross, R. E. Blankenship, Molecular mechanism of photoactivation and structural location of the cyanobacterial orange carotenoid protein. *Biochemistry* **53**, 13–19 (2014). Medline doi:10.1021/bi401539w

30. L. Tian, I. H. van Stokkum, R. B. Koehorst, A. Jongerius, D. Kirilovsky, H. van Amerongen, Site, rate, and mechanism of photoprotective quenching in cyanobacteria. *J. Am. Chem. Soc.* **133**, 18304–18311 (2011). Medline doi:10.1021/ja206414m

31. C. B. de Carbon, A. Thurotte, A. Wilson, F. Perreau, D. Kirilovsky, Biosynthesis of soluble carotenoid holoproteins in *Escherichia coli*. *Sci. Rep.* **5**, 9085 (2015). 10.1038/srep09085 Medline doi:10.1038/srep09085

32. F. X. Cunningham Jr., B. Pogson, Z. Sun, K. A. McDonald, D. DellaPenna, E. Gantt, Functional analysis of the beta and epsilon lycopene cyclase enzymes of Arabidopsis reveals a mechanism for control of cyclic carotenoid formation. *Plant Cell* **8**, 1613–1626 (1996). Medline

33. A. Sedoud, R. López-Igual, A. Ur Rehman, A. Wilson, F. Perreau, C. Boulay, I. Vass, A. Krieger-Liszkay, D. Kirilovsky, The cyanobacterial photoactive orange carotenoid

protein is an excellent singlet oxygen quencher. *Plant Cell* **26**, 1781–1791 (2014). Medline doi:10.1105/tpc.114.123802

34. W. Kabsch, XDS. *Acta Crystallogr. D* **66**, 125–132 (2010). Medline doi:10.1107/S0907444909047337

35. M. D. Winn, C. C. Ballard, K. D. Cowtan, E. J. Dodson, P. Emsley, P. R. Evans, R. M. Keegan, E. B. Krissinel, A. G. Leslie, A. McCoy, S. J. McNicholas, G. N. Murshudov, N. S. Pannu, E. A. Potterton, H. R. Powell, R. J. Read, A. Vagin, K. S. Wilson, Overview of the *CCP*4 suite and current developments. *Acta Crystallogr. D* **67**, 235–242 (2011). Medline doi:10.1107/S0907444910045749

36. F. DiMaio, N. Echols, J. J. Headd, T. C. Terwilliger, P. D. Adams, D. Baker, Improved low-resolution crystallographic refinement with Phenix and Rosetta. *Nat. Methods* **10**, 1102–1104 (2013). Medline doi:10.1038/nmeth.2648

37. P. D. Adams, P. V. Afonine, G. Bunkóczi, V. B. Chen, N. Echols, J. J. Headd, L. W. Hung, S. Jain, G. J. Kapral, R. W. Grosse Kunstleve, A. J. McCoy, N. W. Moriarty, R. D. Oeffner, R. J. Read, D. C. Richardson, J. S. Richardson, T. C. Terwilliger, P. H. Zwart, The Phenix software for automated determination of macromolecular structures. *Methods* **55**, 94–106 (2011). Medline doi:10.1016/j.ymeth.2011.07.005

38. P. Emsley, B. Lohkamp, W. G. Scott, K. Cowtan, Features and development of *Coot*. *Acta Crystallogr. D* **66**, 486–501 (2010). Medline doi:10.1107/S0907444910007493

39. E. F. Pettersen, T. D. Goddard, C. C. Huang, G. S. Couch, D. M. Greenblatt, E. C. Meng, T. E. Ferrin, UCSF Chimera—a visualization system for exploratory research and analysis. *J. Comput. Chem.* **25**, 1605–1612 (2004). Medline doi:10.1002/jcc.20084

40. B. Lee, F. M. Richards, The interpretation of protein structures: Estimation of static accessibility. *J. Mol. Biol.* **55**, 379–400 (1971). Medline doi:10.1016/0022-2836(71)90324-X

41. N. A. Baker, D. Sept, S. Joseph, M. J. Holst, J. A. McCammon, Electrostatics of nanosystems: Application to microtubules and the ribosome. *Proc. Natl. Acad. Sci. U.S.A.* **98**, 10037–10041 (2001). Medline doi:10.1073/pnas.181342398

42. G. E. Crooks, G. Hon, J.-M. Chandonia, S. E. Brenner, WebLogo: A sequence logo generator. *Genome Res.* **14**, 1188–1190 (2004). Medline doi:10.1101/gr.849004

43. S. Gupta, R. Celestre, C. J. Petzold, M. R. Chance, C. Ralston, Development of a microsecond X-ray protein footprinting facility at the Advanced Light Source. *J. Synchrotron Radiat.* **21**, 690–699 (2014). Medline doi:10.1107/S1600577514007000

44. S. Gupta, J. Chai, J. Cheng, R. D'Mello, M. R. Chance, D. Fu, Visualizing the kinetic power stroke that drives proton-coupled zinc(II) transport. *Nature* **512**, 101–104 (2014). Medline

45. A. Marx, N. Adir, Allophycocyanin and phycocyanin crystal structures reveal facets of phycobilisome assembly. *Biochim. Biophys. Acta* **1827**, 311–318 (2013). Medline doi:10.1016/j.bbabio.2012.11.006

46. S. Chaudhury, J. J. Gray, Conformer selection and induced fit in flexible backbone protein-protein docking using computational and NMR ensembles. *J. Mol. Biol.* **381**, 1068–1087 (2008). Medline doi:10.1016/j.jmb.2008.05.042

47. K. Berka, O. Hanák, D. Sehnal, P. Banás, V. Navrátilová, D. Jaiswal, C. M. Ionescu, R. Svobodová Vareková, J. Koca, M. Otyepka, MOLEonline 2.0: Interactive web-based analysis of biomacromolecular channels. *Nucleic Acids Res.* **40**, W222–W227 (2012). Medline doi:10.1093/nar/gks363